Tissue and Cell 84 (2023) 102199

Contents lists available at ScienceDirect

Tissue and Cell

journal homepage: www.elsevier.com/locate/tice

Mesenchymal stem cells differentiate to retinal ganglion-like cells in rat glaucoma model induced by polystyrene microspheres☆☆,☆

Muhsin Eraslan [a,*,1], Eren Çerman [a], Süheyla Bozkurt [b], Deniz Genç [c], Aysın Tulunay Virlan [d], Cansu Subaşı Demir [e], Tolga Akkoç [f], Erdal Karaöz [g,h], Tunç Akkoç [i,j,k]

[a] Department of Ophthalmology, Marmara University Faculty of Medicine, Istanbul, Turkey
[b] Department of Pathology, Marmara University Faculty of Medicine, Istanbul, Turkey
[c] Department of Pediatric Diseases, Faculty of Health Sciences, Muğla Sıtkı Koçman University, Muğla, Turkey
[d] Institute of Infection, Immunity and Inflammation, University of Glasgow, Glasgow, Scotland, UK
[e] Center for Regenerative Medicine and Stem Cell Research & Manufacturing (LivMedCell), Istanbul, Turkey
[f] Genetic Engineering and Biotechnology Institute, Tubitak Marmara Research Center, Kocaeli, Turkey
[g] Department of Histology & Embryology, Istinye University Faculty of Medicine, Istanbul, Turkey
[h] Center for Stem Cell and Tissue Engineering Research & Practice, Istinye University, Istanbul, Turkey
[i] Department of Pediatric Allergy and Immunology, Marmara University Faculty of Medicine, Istanbul, Turkey
[j] Department of Immunology, Marmara University Faculty of Medicine, Istanbul, Turkey
[k] Marstem Cell Technologies, Marmara University Technopark, İstanbul, Turkey

ARTICLE INFO

Keywords:
Glaucoma
Stem cell
Flow cytometry
Polystyrene microsphere
Microbead
Neuro-protection
Neuro-regeneration
Retinal ganglion cell

ABSTRACT

Aim: The study aimed to evaluate the differentiation ability of intravitreally injected rat bone marrow-derived mesenchymal stem cells (rBM-MSCs) to retinal ganglion-like cells in a polystyrene microsphere induced rat glaucoma model.

Materials and Methods: The glaucoma rat model was generated via intracameral injection of 7 microliter polystyrene microspheres. Green fluorescence protein-labeled (GFP) rBM-MSCs were transplanted intravitreally at or after induction of ocular hypertension (OHT), depending on the groups. By the end of the fourth week, flat-mount retinal dissection was performed, and labeled against Brn3a, CD90, GFAP, CD11b, Vimentin, and localization of GFP positive rBM-MSCs was used for evaluation through immunofluorescence staining and to count differentiated retinal cells by flow cytometry. From 34 male Wistar albino rats, 56 eyes were investigated.

Results: Flow cytometry revealed significantly increased CD90 and Brn3a positive cells in glaucoma induced and with rBM-MSC injected groups compared to control($P = 0.006$ and $P = 0.003$ respectively), sham-operated ($P = 0.007$ and $P < 0.001$ respectively), and only rBM-MSCs injected groups ($P = 0.002$ and $P = 0.009$ respectively). Immunofluorescence microscopy revealed differentiation of GFP labeled stem cells to various retinal cells, including ganglion-like cells. rBM-MSCs were observable in ganglion cells, inner and outer nuclear retinal layers in rBM-MSCs injected eyes.

Conclusion: Intravitreally transplanted rBM-MSCs differentiated into retinal cells, including ganglion-like cells, which successfully created a glaucoma model damaged with polystyrene microspheres. Promisingly, MSCs may have a role in neuro-protection and neuro-regeneration treatment of glaucoma in the future.

1. Introduction

Glaucoma is one of the significant causes of blindness. It is regarded as progressive optic neuropathy, characterized by degeneration of retinal ganglion cells (RGCs) associated with elevated intraocular pressure (IOP) (Yap et al., 2020). Although age is the most significant risk factor, (Mohammadzadeh et al., 2021) current glaucoma therapies are focused on reducing IOP because IOP is the only commutable risk factor

☆☆ Study Conducted: Marmara University Faculty of Medicine. ☆ This manuscript has not been published and is not under consideration for publication elsewhere.

* Correspondence to: Marmara Universitesi Pendik Egitim Arastirma Hastanesi, Goz Hastaliklari Anabilim Dali Departmani, Fevzi Cakmak Mah, Muhsin Yazicioglu Cad. No: 10 Ust Kaynarca, Pendik, Istanbul, Turkey.
E-mail address: muhsineraslan@hotmail.com (M. Eraslan).
[1] ORCID ID: 0000–0002-1829–3329

https://doi.org/10.1016/j.tice.2023.102199
Received 6 March 2023; Received in revised form 17 August 2023; Accepted 17 August 2023
Available online 19 August 2023

for the progression of the disease (Gordon and Kass, 2018). However, despite maximally tolerated ocular hypotensive therapy, progressive loss on the visual field continues in a proportion of patients, suggesting that IOP independent mechanisms may also play a role in glaucomatous degeneration (Johnson et al., 2010). Thus, investigations of novel therapies which protect RGCs from deterioration have gained consideration (Emre et al., 2015; Lai et al., 2010).

Mesenchymal stem cells (MSCs) are considered as multipotent adult progenitor cells and they have the capacity to self-renew and differentiate into various cell lineages. The source of MSC are various as bone marrow, umbilical cord, and adipose tissues (Ding et al., 2011). Recent laboratory and clinical studies show that MSCs have considerable potential in cellular immunotherapy for the treatment of a number of autoimmune, atopic and inflammatory disorders (Laing et al., 2018; Akkoc and Genc, 2020; Girdlestone, 2016).

Previous studies revealed that local transplantation of autologous rat bone marrow mesenchymal stem cells (rBM-MSCs) have significant neuroprotective effects on RGCs in several central nervous system degenerative disease models and glaucoma models. Still, systemic stem cell delivery is shown to be less effective as a treatment modality for glaucoma in rat models (Johnson et al., 2010; Khine et al., 2020; Parr et al., 2007; Slavin et al., 2008; Torrente and Polli, 2008) This finding reveals the need for further investigations on intravitreal autologous rBM-MSCs transplantation, which may help to show the true potential of these neuroprotective therapies (Johnson et al., 2010).

Clinical and experimental studies have shown that many types of stem cells are effective in neuroprotection, cell replacement, (Hau et al., 2021) (Bunce and Wormald, 2006) and regeneration. (Yoshii et al., 2007) rBM-MSCs are attractive candidates for cell-based neuroprotective therapies because they may provide an autologous approach and can be isolated from various tissues, including adult bone marrow. (Johnson et al., 2010) It is suggested that they may transdifferentiate into neural cells, although this remains controversial. (Krabbe et al., 2005) Recent studies have revealed that MSCs may produce and secrete both neurotrophic factors and anti-inflammatory cytokines in situ after transplantation, which may produce neuroprotective effects in models of neurodegenerative disease (Puertas-Neyra et al., 2020; Usategui--Martin and Fernandez-Bueno, 2021; Jin et al., 2008; Joyce et al., 2010; Kim et al., 2009; Vercelli et al., 2008; Zappia et al., 2005; Zhang et al., 2009; Zhao et al., 2007).

Rats are the most commonly used rodent species for inducing ocular hypertension, mostly by altering aqueous fluid dynamics in the anterior segment. (Liu et al., 2020; Pang and Clark, 2007) Most ocular hypertension (OHT) models are limited by the absence of a repeatable internal control. An equivalent insult in the fellow eye would not result in extended elevated IOP. Sappington et al., (2010) established a rodent model of OHT with an injection of small volumes of polystyrene microspheres into the anterior chamber to impede aqueous outflow by occluding the trabecular meshwork elevating IOP. (Sappington et al., 2010) They constructed this model on a limited number of previous reports using microspheres to elevate IOP.(Ngumah et al., 2006; Urcola et al., 2006; Weber and Zelenak, 2001) Intracameral injection of polystyrene microspheres establishes sustained and moderate elevation of intraocular pressure, which can be initiated at precise time points, and both IOP magnitude and duration can be manipulated, which makes this model have the most similar pathophysiology to the human OHT mechanism and has evolved as a preferred method of IOP elevation in rodents (Liu et al., 2020; Calkins et al., 2018; Morgan and Tribble, 2015; Sappington et al., 2010).

This study investigated the differentiation of intravitreally injected rBM-MSCs to retinal ganglion-like cells in a rat glaucoma model induced with anterior chamber polystyrene microsphere injection. We examined the migration of green fluorescein protein (GFP)-labeled rBM-MSCs into the retina by immunofluorescence and assessed the number of differentiated retinal cells using flow cytometry.

2. Materials & methods

2.1. Animals

In this study, reproduction of animals, intracameral microsphere injections, intravitreal MSC transplantations, euthanizing of the animals, and preparation of samples for immunofluorescence microscopy and flow cytometry were performed at the Experimental Animal Laboratory of Marmara University (Istanbul, Turkey). Immunohistochemistry was conducted in the pathology laboratory of Marmara University Institute of Neurosciences. Immunofluorescence studies were carried out at the Kocaeli University Centre for Stem Cell and Gene Therapies Research and Practice. Ethics approval was granted by the Ethics Committee for Animal Experimentation of Marmara University, Istanbul, Turkey, and complies with the ARVO Statement for the Use of Animals in Ophthalmic and Vision Research (242013MAR).

A total of 34 adult 12-week-old male Wistar albino rats with a bodyweight of about 200–250 g were used in the study. They were maintained in a room under controlled environmental conditions of humidity and temperature (21 °C ± 2 °C) with 12-hour light/dark cycles. The subjects were kept in standard cages in groups (four subjects per group) and were fed with a regular rat pellet diet and water available ad libitum. Sacrificing was maintained using overdose anesthetics.

Eyes with an IOP over 21 mmHg, 24 h after the intracameral injection of 7 μl (1×10^6) polystyrene microspheres to the anterior chamber were diagnosed as OHT; animals which did not fulfil this criterion were excluded. The right and left eyes of rats were used in separate study groups to decrease the number of animals:

The right eyes of rats (n = 10) were used as the **Control group (CONTROL),** and the left eyes with induced OHT were enrolled into the **Glaucoma-Sham group (G-SHAM)**. Two weeks after induction of OHT, 2 μl Balanced Salt Solution (BSS) (Miray Medikal, Bursa, Turkey) was intravitreally applied to the left eyes, and the animals were euthanized at the 4th week.

OHT was initially induced in the left eyes, and after two weeks, 2 μl solution containing 200×10^3 GFP labeled rBM-MSCs was intravitreally transplanted to both eyes. The right eyes were called as **MSC group (n = 12) (MSC) and the left eyes as the Glaucoma-MSC group (G-MSC)**. Animals were euthanized after two weeks of rBM-MSCs application.

In the remaining 12 rats, 2 μl solution containing 200×10^3 GFP labeled rBM-MSCs was intravitreally transplanted, and OHT was induced at 14. day concurrently with rBM-MSCs transplantation in the left eyes and these eyes were labeled as the **Concurrent-Glaucoma-MSC group (C-G-MSC).** Only the left eyes were included in the study, while the right eyes were excluded to avoid double organ bias. (Esen et al., 2016) Animals were sacrificed four weeks after the induction of OHT.

Following the sacrificing process, the eyes were collected, and Brn3a, CD90, GFAP, Rhodopsin, CD11b, Vimentin, and localization of GFP positive rBM-MSCs were analyzed with immunofluorescence and flow cytometry.

2.2. Characterization and labelling method of rat bone marrow-derived mesenchymal stem cell culture

Wistar albino rats were sacrificed by an overdose of hydrochloride and xylazine. Cancellous bone marrow from the femur and tibias were collected and washed with RoboSep buffer (Stem Cell Technologies, Vancouver, BC, Canada), which is achieved by drawing and expelling the sample several times with a syringe. The compact bones were minced to fine chips of about 1 mm^3 in plastic culture dishes, equilibrated in Dulbecco's phosphate-buffered saline (DPBS) containing 20% fetal bovine serum (FBS) and 0.25% collagenase type I (Stem Cell Technologies, Vancouver, BC, Canada). The samples were placed in a shaking water bath for 45 min at 37 °C. The freed cells were aspirated, and RoboSep buffer was used to wash the bone fragments three times.

The cells were centrifuged at 300g for 10 min, and a cell pellet was re-suspended in RoboSep culture medium, which contained PBS + 2% FBS + 1 mM EDTA (Stem Cell Technologies, Vancouver, BC, Canada) and the EasySep™ mouse mesenchymal stem/progenitor cell enrichment kit (Stem Cell Technologies, Vancouver, BC, Canada) were used in isolation of rBM-MSCs by negative selection according to the manufacturer's instructions. As a next step, rBM-MSCs were re-suspended in the MesenCult proliferation medium and plated in T25 flasks at 37 °C in a humidified atmosphere of 5% CO_2. The medium was refreshed every four days. 0.25% trypsin–EDTA (Gibco®; Thermo Fisher Scientific, Waltham, MA, USA) was used to separate rBM-MSCs when they reached 70–80% confluence. rBM-MSCs were characterized using flow cytometry analysis of relevant specific stem cell surface markers.

After cell homogenization, the samples were transferred to polystyrene tubes. For positive and negative surface markers, we employed specific monoclonal antibodies conjugated with fluorescent isothiocyanate (FITC), phycoerythrin (PE), and allophycocyanin (APC). The antibodies used in this study for the characterization of MSCs were ready-to-use antibodies obtained from BD Biosciences, UK. For positive surface markers, we used CD73 PE, CD146 FITC, CD105 PE, and CD29 APC. On the other hand, the negative surface markers employed were CD3 PE, CD14 FITC, CD34 APC, and CD20 PE." As controls, isotype antibodies (mouse IgG1 from BD Biosciences, San Diego, CA) used. All samples were introduced and allowed to incubate for 30 min at ambient temperature shielded from light. Post-incubation, the samples were treated with DPBS and then centrifuged for 5 min at 1200 rpm. The supernatant was discarded, followed by addition and resuspension in a cell-washing solution. The final cell suspension was then analyzed using a FACS Calibur flow cytometer from BD, San Jose, CA.

2.3. OHT induction with polystyrene microsphere injection

Before injections, animals were anesthetized with intraperitoneally administered ketamine hydrochloride (25 mg/kg; Ketalar, Pfizer) and xylazine hydrochloride (10 mg/kg; Rompun, Bayer). Pupils were dilated with 1% tropicamide ophthalmic solution (Bausch & Lomb, Tampa, FL), and anesthetic drops (0.5% proparacaine hydrochloride; Bausch & Lomb) were applied to each eye. After dilation of the iris and protraction of the eye with forceps, OHT was induced by intracameral injections of 7 μl (1×10^6) polystyrene microsphere suspension, which contains sterile micro-particles based on polystyrene with a dimension of 15 μm (product:74964, Sigma Aldrich Co., St. Louis, MO, USA), using a 34-gauge NanoFil syringe (World Precision Instruments, Sarasota, USA). The injections were made through the corneal limbus into the anterior chamber to create a self-sealing entry under a surgical microscope, using a micromanipulator to position the needle in the anterior chamber approximately 3 mm central to the ora serrata. The needle was moved in a clockwise direction to avoid lens and iris touch (Calkins et al., 2018; Moreno et al., 2005).

After injection, antibiotic drops (0.5% moxifloxacin hydrochloride ophthalmic solution; Alcon, Fort Worth, TX) were placed on each eye. The animal was allowed to recover 24 h before resumption of IOP measurements. After 24 h, IOP rates were monitored with a tonometer (Tono-Pen Avia; Reichert, Inc.). Tonometry was performed within 5–10 min of initiation of anesthesia and always between 10:00 am, and 11:30 am. Rats with two consecutive IOP measurements higher than 21 mmHg at the same examination were diagnosed with OHT.

2.4. Intravitreal stem cell injection

20 μl solution containing 2×10^5 rBM-MSCs was intravitreally injected with a 30-gauge needle, HA (Sigma) under general anesthesia, which was induced by intraperitoneal administration of ketamine hydrochloride (25 mg/kg; Ketalar, Pfizer) and xylazine hydrochloride (10 mg/kg; Rompun, Bayer) and a drop of topically applied proparacaine HCl (Alcaine, Alcon). The intravitreal injections of rBM-MSCs were performed under a binocular stereomicroscope (Tronic XTX 3 C, Beijing People's Republic of China) through the 1 mm posterior to the limbus. The solution was injected slowly and progressively.

2.5. Flow cytometry analysis of retinal cell suspensions

Retinal cells were analyzed via a flow cytometer (FacsCalibur). To prepare retinal cell suspensions, tissues were dissociated in Eagles's MEM solution containing 20 U/ml papain, 1 mM L-cysteine, 0.5 mM EDTA, and DNase (0.005%), (Worthington, Lakewood, NJ) at 37 °C for 40 min. The retinas were then rinsed in an inhibitor solution containing Eagle's minimum essential medium, ovomucoid (0.2%) (US Biological, Swampscott, MA), DNase (0.04%), and bovine serum albumin (0.1%) (Sigma, St. Louis, MO). At the end of the incubation period, tissues were triturated through a 1 ml plastic pipette to yield a suspension of single cells. The retinal cells were centrifuged at 400g for 10 min and re-suspended in phosphate-buffered saline solution. The total number of dissociated retinal cells counted in separate experiments using 10 rats was $1.86 \pm 0.56 \times 10^6$ per rat eye. Cell suspensions were separately incubated with *Antibodies* labeled with fluorochromes (BD Biosciences, San Jose, CA) and analyzed for surface markers of CD90 (Phycoerythrin, PE), Brn3a (Allophycocyanin, APC), CD11b (Phycoerythrin, PE). GFP labeled cells were analyzed by using the fluorescein isothiocyanate (FITC) channel.

2.6. Histology

The rats were deeply anesthetized with ketamine hydrochloride (100 mg/kg) and xylazine (5 mg/kg), and they were intracardially perfused with 4% paraformaldehyde. Their eyes were enucleated and immersion fixed overnight in 4% paraformaldehyde in PBS (pH 7.4) at 4 °C. They were subsequently dehydrated over several hours and embedded in paraffin in a transverse orientation.

2.7. Immunohistochemistry

Four-micrometer-thick sections were placed on 3-aminopropyletxylene-covered slides and deparaffinized at 60 °C for 1 h. The slides were dewaxed in xylene and dehydrated in 96% alcohol. Sections were then immersed in 10 mmol/l citrate buffer (pH 6.0) and microwaved for 20 min for antigen retrieval. Slides were cooled to room temperature and rinsed in phosphate-buffered saline (PBS). Endogenous peroxidase activity was blocked by further pre-treatment with 3% H_2O_2 / distilled water for 20 min at room temperature. After thorough washing in PBS, a blocking solution (ScyTek Laboratories, Logan, Utah USA) was applied to block nonspecific antibody binding (5 min). The sections were incubated with GFAP (1/100, clone GA5, Leica, Novocastra, Newcastle, United Kingdom), NFP (1/100, clone 2F11, GENEMED, South San Francisco, CA 94080 USA), MBP (Cell Marque, LLC. Sigma-Aldrich Co., LLC is a subsidiary of Merck KGaA, Darmstadt, Germany. clone Rabbit Polyclonal, ready to use) rabbit monoclonal for 1 h at RT. After a 10-min rinsing in PBS, biotinylated goat anti-polyvalent immunoglobulin (ScyTek Laboratories, Logan, Utah USA) for 20 min, and in the streptavidin-biotin peroxidase complex (ScyTek Laboratories, Logan, Utah USA) for 20 min being applied at RT, 3,3diaminobenzidine chromogen (ScyTek Laboratories, Logan, Utah USA) for 5 min was used for visualization of antigen-antibody binding. The sections were counterstained with hematoxylin, dehydrated, cleared in xylene, and mounted on Entellan coverslips. The normal brain sections were used as a positive control for GFAP and NFP. Negative controls were performed omitting the primary antibodies.

2.8. Immunofluorescence

To detect GFP-labelled BMSC, paraffin-embedded sections were twice deparaffinized with xylene for five minutes and rehydrated in a

series of graded alcohol solutions (70–100%). Endogenous peroxidases were inhibited by incubation with 3% H_2O_2 in PBS buffer. For antigen retrieval, the samples were heated to 98–99 °C in antigen-retrieval buffer (10 mMTri-sodium citrate, 0.05% Tween 20, pH 6.0) and incubated for 30 min in the pressurized vessel. Nonspecific staining was blocked with a mixture of sera in 1.5%PBS for 30 min at room temperature and incubated in the mix of two primary antibodies in a pairwise fashion with the mouse monoclonal anti-GFP antibody (SC-9996) at 1:50 dilutions for 1 h at room temperature. Following incubation with the appropriate fluorescent-conjugated secondary antibodies, the sections were covered with a mounting medium containing DAPI (Santa Cruz, Heidelberg, Germany). The cells were investigated under a fluorescence microscope (Leica DMI 4000B; Leica Microsystems, Wetzlar, Germany). For other immunostainings, the following antibodies were supplied from Abcam (Cambridge, MA, USA): GFAP (ab4674), anti-vimentin antibody (ab8979), and BRN3A (ab81213). The dilution rate of all primary antibodies was 1:100.

2.9. Statistics

Data were expressed as the mean ± standard error of the mean (SEM), and they were analyzed using SPSS (Statistical Package for the Social Sciences) software version 17.0 (IBM Corporation, Armonk, NY, USA). The standard *t*-test was used with a significance level of $P < 0.05$. Shapiro–Wilk's test ($P > 0.05$) was performed. A visual inspection of the histograms, Q-Q plots, box plots, skew, and kurtosis was undertaken for both the preoperative and postoperative data to differentiate between normal and non-normal distributions. For normally distributed data, the

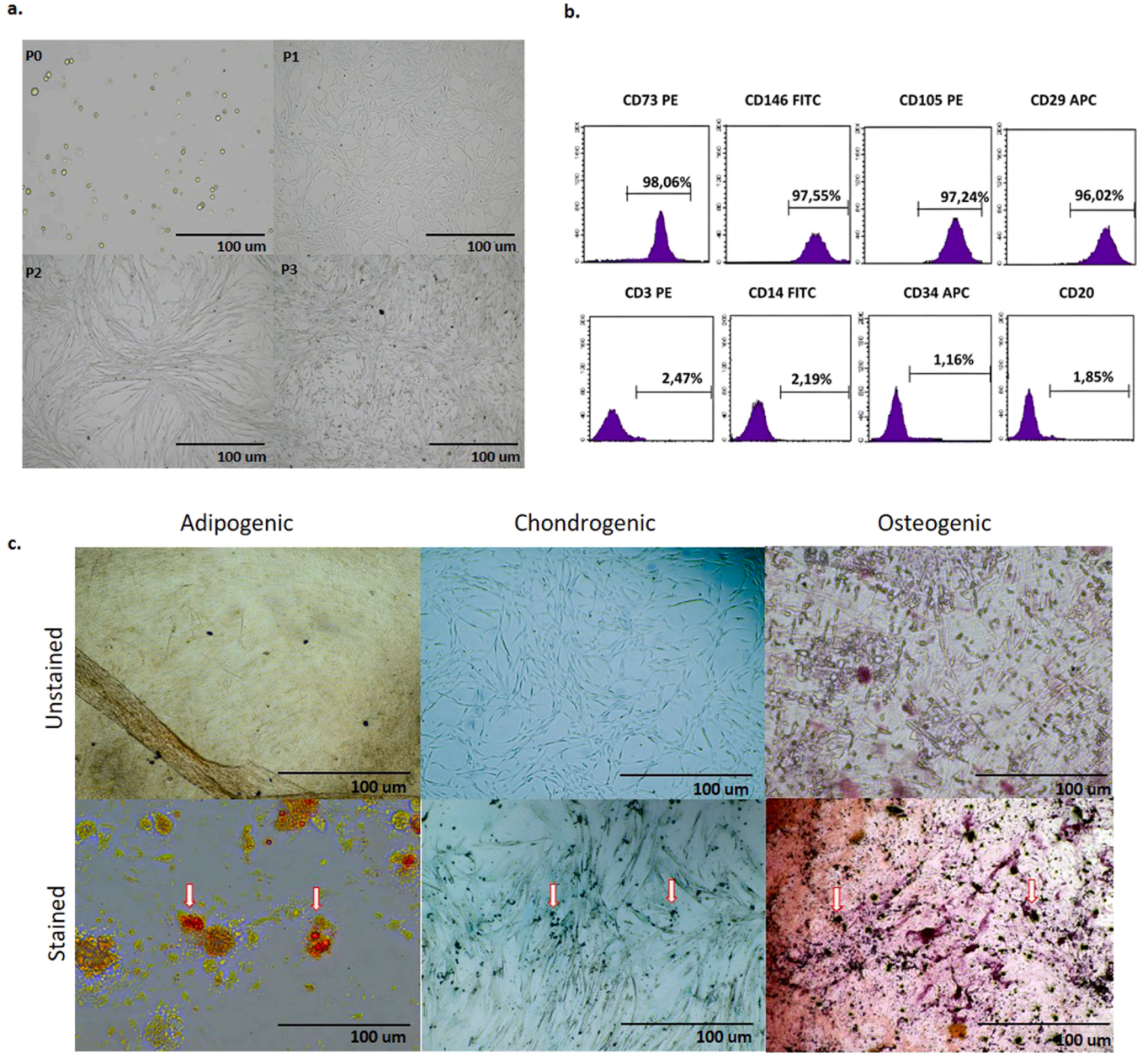

Fig. 1. Isolation, Characterization, and Multipotency of rBM-MSCs. a) Morphologically, fibroblast-like colonies formed by rBM-MSCs with 80–90% confluency in 6–8 days after being plated. (P1, P2, P3: First, second, third passage, respectively) b) Flow cytometry analysis of the surface markers. Positive markers for CD29, CD73, CD105, and CD146 were negative for CD14, CD34, CD3, and CD20. c) The adipogenic differentiation was evaluated using Oil Red O and hematoxylin-eosin staining. The chondrogenic differentiation potential was confirmed with Alcian blue staining. The osteogenic differentiation capability of rBM-MSCs was shown using Alizarin red, and calcium deposits were stained in light red color.

paired *t*-test for within-group comparisons and the unpaired *t*-test for between-group comparisons were used. For non-normal distributions, within-group comparisons were made with Wilcoxon's paired test, and between-group comparisons were made with the Mann–Whitney U test. Kruskal Wallis test was used to compare multiple groups.

3. Results

3.1. Isolation, characterization, and multipotency of rBM-MSCs

rBM-MSCs attached and formed colonies with fibroblast-like morphology in the culture flasks during the early days of the incubation period and reached 80–90% confluency in 6–8 days after being plated (Fig. 1a). In the third passage, immunophenotyping and differentiation potential of cell lineages were examined.

The surface markers of rBM-MSCs were analyzed by flow cytometry. These cells were evaluated with positive markers for CD29, CD73, CD105, and CD146 and were negative for CD14, CD34, CD3, and CD20 (Emre et al., 2015) (Fig. 1b).

rBM-MSCs were differentiated into osteocytes, adipocytes, and chondrocytes. The osteogenic differentiation capability was investigated in vitro during a twenty-one-day culture period in an osteogenic induction medium. rBM-MSCs were stained with Alizarin red, and calcium deposits were stained in light red color. The adipogenic differentiation was evaluated by culturing the cells in an adipogenic induction medium for fourteen days and Oil Red O and hematoxylin-eosin staining. Intracellular oil droplets were observed at the end of the culture period. The chondrogenic differentiation potential was evaluated by culturing with chondrogenic stimulation for fourteen days and chondrocytes were confirmed with Alcian blue staining (Fig. 1c).

3.2. Intraocular pressure induction

Mean IOP values were similar among all groups before the induction of OHT. ($P > 0.05$) Intraocular pressure (IOP) increased significantly within 24 h following polystyrene microsphere injections into the anterior chamber until the end of the 2nd week. It then began to decrease, which yielded a statistically significant intragroup change ($P < 0.001$). (Table 1) (Fig. 2) Significantly higher mean IOP values were measured in OHT induced eyes compared to the Control and MSC groups ($P < 0.001$). There was no significant difference between IOP values of the OHT induced groups during all examinations ($P > 0.05$), which shows that the number of RGC seems to be linked to the treatment.

3.3. Morphological and immunohistochemical findings

3.3.1. Control group

Histological sections of the optic nerve in the control group revealed no morphologic alterations. Glial cells are scattered in number, and they are oriented in columns parallel to the course of the nerve fiber. (Fig. 3A1) GFAP (Glial fibrillary acidic protein) immunohistochemistry demonstrated faint expression in glial cells of the optic nerve. (Fig. 3A2) Neurofibrillary protein (NFP) immunohistochemistry shows homogeneously distributed axonal fibers. (Fig. 3A3).

3.3.2. G-Sham group

Histological sections of the optic nerve in the GBSS group revealed degenerated swollen axons and vacuolization in myelin. (Fig. 3B1) Glial cells are found to be increased in number and are distributed haphazardly throughout the optic nerve. GFAP immunohistochemistry demonstrated glial hypertrophy with increased expression in glial cells of the optic nerve. (Fig. 3B2) NFP immunohistochemistry shows enlarged axonal fibers with intense staining. (Fig. 3B3).

3.3.3. G-MSC group

Histological sections of the optic nerve in the G-MSC group revealed degenerated axons and vacuolization in myelin. (Fig. 3C1) Glial cells are found to be increased in number and distributed haphazardly throughout the optic nerve. GFAP immunohistochemistry demonstrated glial hypertrophy with increased expression in glial cells of the optic nerve. (Fig. 3C2) NFP immunohistochemistry shows enlarged axonal fibers with intense staining. (Fig. 3C3).

3.3.4. MSC group

Histological sections of the optic nerve in the MSC group revealed mild morphologic alterations. Glial cells are found to be scattered in number and oriented in columns parallel to the course of the nerve fiber. (Fig. 3D1) GFAP immunohistochemistry demonstrated faint expression in glial cells of the optic nerve. (Fig. 3D2) NFP immunohistochemistry shows increased intensity in some of the axonal fibers. (Fig. 3D3).

3.3.5. C-G-MSC group

Histological sections of the optic nerve in the C-G-MSC group revealed vacuolization in myelin and degeneration in axons. (Fig. 3E1) Glial cells, which are distributed haphazardly throughout the optic nerve, were found to be increased in number. GFAP immunohistochemistry demonstrated glial hypertrophy with increased expression in glial cells of the optic nerve. (Fig. 3E2) NFP immunohistochemistry shows enlarged axonal fibers with intense staining (Fig. 3E3).

Histological evaluation of OHT induced eyes revealed an increased amount of vacuolization in myelin, glial, and neurofibrillary reactions, which confirm the achievement of glaucomatous degeneration.

3.4. Flow cytometry identification results

OHT induced left eyes were subjected to flow cytometry analysis for GFP labelled rBM-MSCs ($CD90^{+}GFP^{+}$), differentiation of $CD90^{+}$ cells to vimentin expressing cells ($CD90^{+}Brn3a^{+}$), differentiation of GFP labelled cells to vimentin expressing cells ($Brn3a^{+}GFP^{+}$), differentiation of GFP labelled cells to CD11b expressing cells ($CD11b^{+}GFP^{+}$), and vimentin expressing $CD11b^{+}$cells ($CD11b^{+}Brn3a^{+}$).

Table 1
Statistical analysis of intraocular pressure at preoperative, day 1 and 2, week 1, 2, 3, and 4.

	IOP (Mean ± SD)							
Groups	Preop (mmHg)	1. Day (mmHg)	2. Day (mmHg)	7. Day (mmHg)	13. Day (mmHg)	2. Week (mmHg)	3. Week (mmHg)	4. Week (mmHg)
Control	12.20 ± 1.5	12.20 ± 1.40	12.10 ± 1.6	12.40 ± 1.2	12.30 ± 1.2	12.40 ± 1.7	12.30 ± 1.1	12.30 ± 1.8
MSC	12.10 ± 2.0	12.42 ± 1.1	12.58 ± 1.6	12.80 ± 1.6	12.65 ± 1.0	13.00 ± 2.0	12.90 ± 1.5	12.33 ± 1.8
G-Sham*	12.10 ± 1.3	24.90 ± 3.6	27.50 ± 3.2	26.90 ± 3.1	24.10 ± 2.2	23.50 ± 2.5	18.60 ± 3.5	15.00 ± 3.3
G-MSC *	12.50 ± 1.9	26.25 ± 4.3	28.92 ± 3.5	28.25 ± 3.5	24.67 ± 2.7	23.92 ± 2.8	19.08 ± 3.5	16.75 ± 2.7
C-G-MSC *	12.13 ± 1.6	-	-	-	-	27.08 ± 3.7	27.50 ± 3.8	29.08 ± 3.3
P Value	0.960	< 0.001	< 0.001	< 0.001	< 0.001	< 0.001	< 0.001	< 0.001

Control group (CONTROL), MSC group (MSC), Glaucoma-Sham group (G-SHAM), Glaucoma-MSC group (G-MSC), and Concurrent-Glaucoma-MSC group (C-G-MSC) — Glaucoma was inducted at 2.week.
(*) character and boldly written P values indicate the statistically significant difference with the Control group.

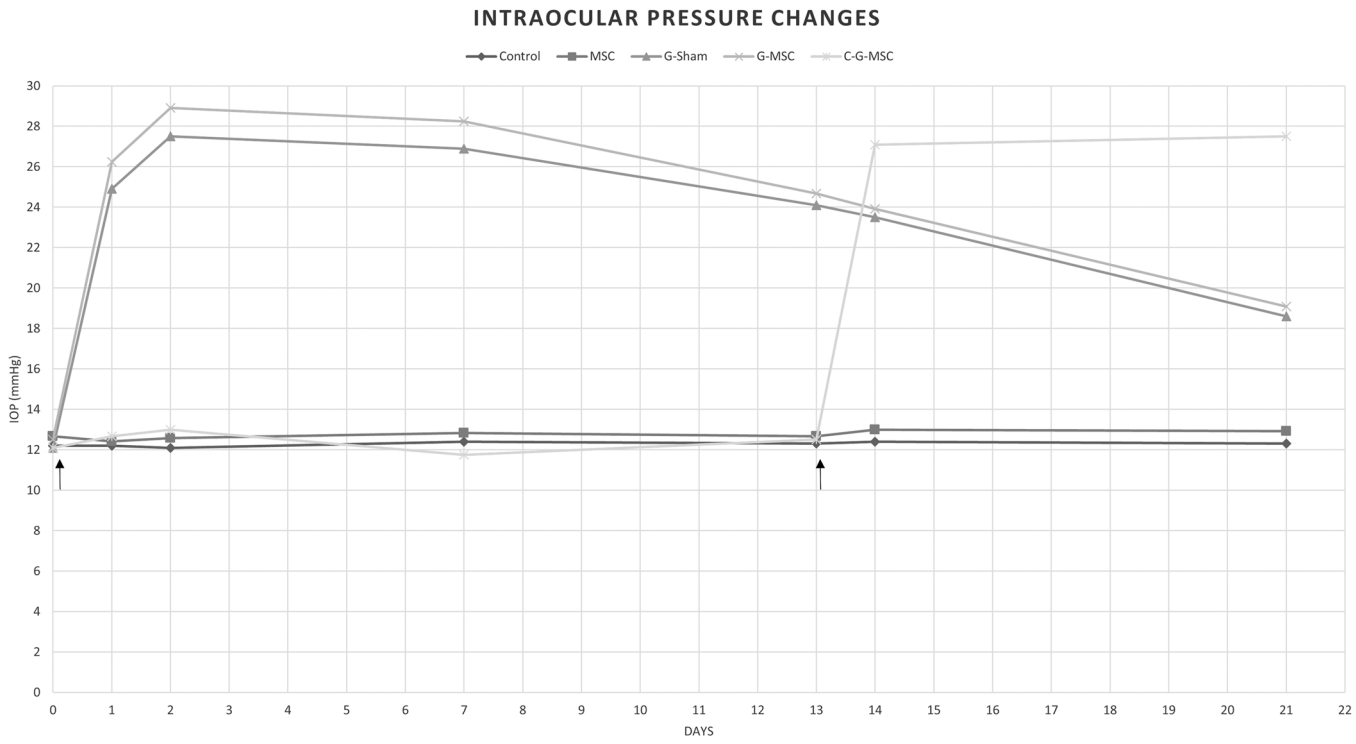

Fig. 2. Daily changes of intraocular pressure of all groups. The first arrow shows the time of intraocular pressure induction of G-Sham and G-MSC groups, and the second arrow shows the C-G-MSC group.

$CD90^{+}GFP^{+}$ cells were significantly high in the MSC (2.48 ± 0.12), C-G-MSC (2.27 ± 0.08), and G-MSC (2.35 ± 0.29) groups compared to the control groups (1.42 ± 0.27, $P = 0.007$, $P = 0.006$ and $P = 0.03$, respectively) and the G-Sham groups (1.38 ± 0.17, $P = 0.008$, $P = 0.005$ and $P = 0.007$), which shows that injected GFP labelled cells were located in rodent retinas (Table 2 and Fig. 4a).

$CD90^{+}Brn3a^{+}$ cells were found to be significantly increased in the C-G-MSC (3.89 ± 0.52) and G-MSC (4.26 ± 0.18) groups compared to the control (1.30 ± 0.41, $P = 0.006$ and $P = 0.003$ respectively), sham operated (0.90 ± 0.05, $P = 0.007$ and $P < 0.001$ respectively), and MSC group (1.96 ± 0.03, $P = 0.002$ and $P = 0.009$ respectively) (Table 2 and Fig. 4b).

The frequency of $Brn3a^{+}GFP^{+}$ and $CD11b^{+}GFP^{+}$ cells notably increased in the G-MSC group compared to the other groups ($P = 0.03$). Still, no significant difference was found in the C-G-MSC group compared to the control, G-Sham, and only MSC injected groups ($P = 0.06$) (Table 2 and Fig. 4c, 4.d).

3.5. *Immunofluorescence results*

Immunofluorescence study results showed integration of rBM-MSCs into the retina and transdifferentiation to ganglion-like (GFP-Brn3a positive) cells (Fig. 5).

Immunofluorescence staining of the MSC group, G-MSC, and C-G-MSC groups at the 2nd week of transplantation revealed that GFP labeled rBM-MSCs were integrated into ganglion cell layer, inner and outer nuclear layers. (Figs. 5 and 6) The rBM-MSCs transplanted retinal sections were positive for both GFP and Brn3a (intracellular ganglion cell marker, Fig. 5) or vimentin (MSC marker; Fig. 6). The GFP and MSCs marker vimentin co-staining indicated that the origin of these cells were rBM-MSCs used in transplantation. The GFP and intracellular ganglion cell marker (Brn3a) co-staining was interpreted as the trans-differentiation of the rBM-MSCs to retinal ganglion-like cells. The retinal sections of the G-MSC group showed more intense staining compared to the C-G-MSC group regarding GFP-BRN3A and GFP-Vimentin. And MSC group showed less staining compared to other MSCs injected groups. Control and G-Sham groups did not show any staining. (Fig. 6) Some GFP-labeled cells were seen as located in the outer nuclear layer. (Fig. 6) No tumor formation was determined throughout this study.

4. Discussion

The present study demonstrated that intravitreally transplanted rBM-MSCs could integrate into the retinal layers and differentiate to ganglion-like cells, which may lead to neuroprotection in a rat model of glaucoma. Our previous study supported this finding, which showed intravitreally transplanted rBM-MSCs could protect RGCs from diabetic retinopathy in which GFP labeled intravitreally transplanted rBM-MSCs were integrated into the retinal layers. The ERG results confirm that these cells have neuroprotective and functional effects in restoring vision (Cerman et al., 2016).

Traditional methods currently being used to estimate the total retinal ganglion cell number rely on cell counts in different microscopic fields of the flat-mounted or sectioned retinas. (Yang et al., 2000) However, technical difficulties and partial sampling limit the informative value of these experiments. These methods typically employ counts of only up to 25% of the RGC population due to differences in the regional distribution of RGCs. (Aydin et al., 2021; Yang et al., 2000) Flow cytometry applies high-content analytical technology to evaluate multiple biochemical and morphological properties in a single cell. Flow cytometry uses previously specified antibodies that target a specific structural component of a particular cell type during the cell count. In the present study, we used flow cytometry for simple, rapid, and correct counting of all labeled retinal cells individually, including RGCs.

During the current study, the optic nerve damage was assessed using immunohistochemical staining, which revealed the glaucomatous degeneration as increased glial and neurofibrillary reaction and vacuolization in myelin. Survival of RGC bodies within the retina was quantified directly using flow cytometry. Immunofluorescence staining of

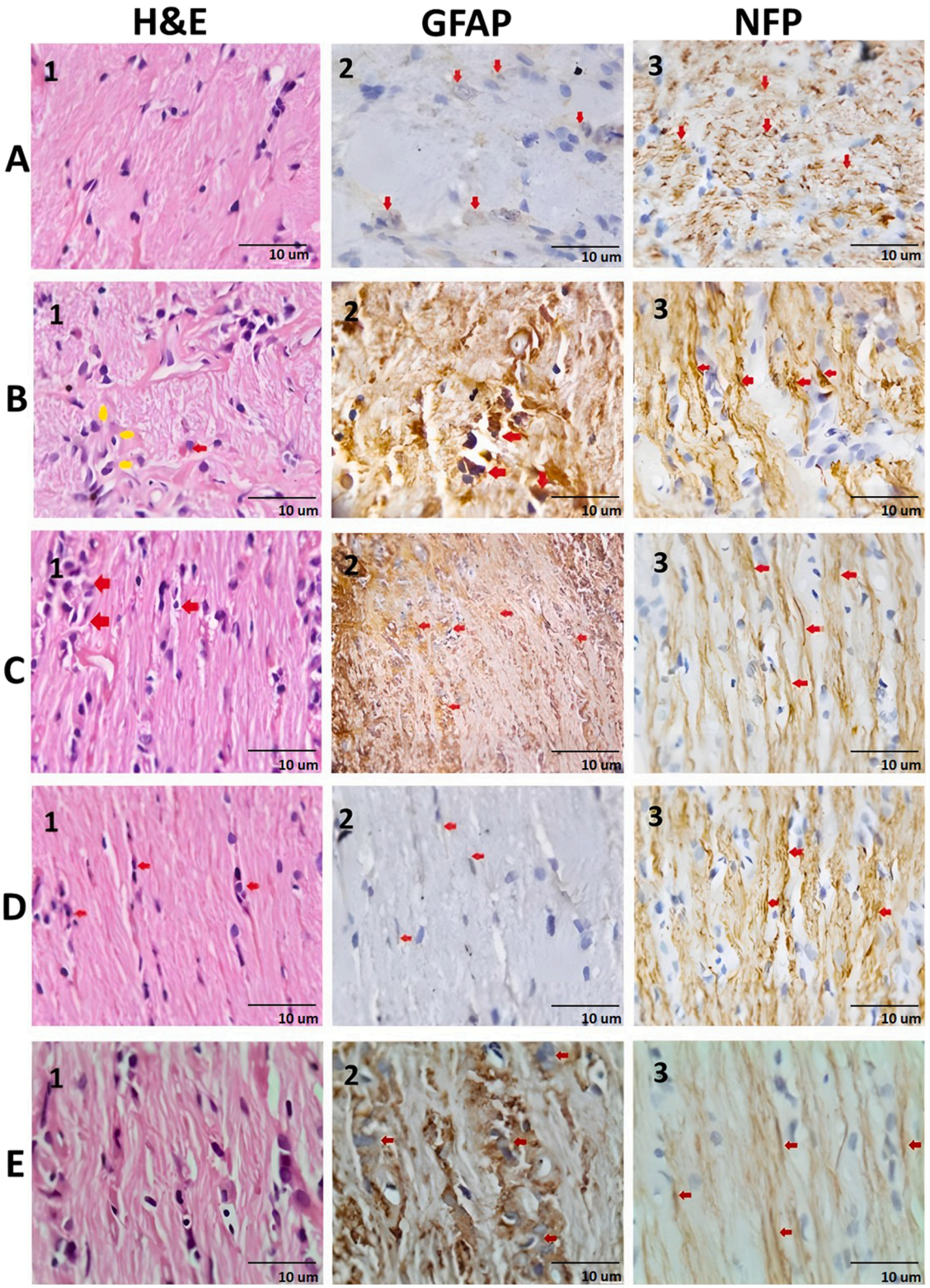

(caption on next page)

Fig. 3. Histological sections of the optic nerve. H&E: hematoxylin and eosin; GFAP: Glial fibrillary acidic protein, NFP: Neurofibrillary Protein. Arrows showing glial cells in the images of GFAP and axonal fibers in the images of NFP used sections. *Control Group* A1: Histologic sections of optic nerve demonstrating no morphological alteration. (H&E, x 100 magnification). A2: Faint GFAP immunoreactivity in astrocytes of the optic nerve (red arrows). (GFAP, x100 magnification). A3: Homogeneously distributed NFP stained axonal fibers are seen in the optic nerve (red arrows) (NFP, x100 magnification). *G-Sham Group* B1: Histologic sections of optic nerve demonstrating degenerated swollen axons (red arrow) and increased number of glial cells (yellow arrows) (H&E, x 100 magnification). B2: Hypertrophy and increased expression of GFAP immunoreactivity in astrocytes of the optic nerve (red arrows). (GFAP, x100 magnification). B3: Intensified axonal staining of NFP are seen in the optic nerve (red arrows) (NFP, x100 magnification). *G-MSC Group* C1: Histologic sections of optic nerve demonstrating vacuolization and increased number of glial cells (red arrows), (H&E, x 100 magnification). C2: Hypertrophy and increased expression of GFAP immunoreactivity in astrocytes of the optic nerve (red arrows). (GFAP, x100 magnification). C3: Intensified axonal staining of NFP are seen in the optic nerve (red arrows) (NFP, x100 magnification). *MSC Group* D1: Histologic sections of optic nerve demonstrating minimal morphological alteration. glial cells (red arrows), (H&E, x 100 magnification). D2: Faint GFAP immunoreactivity in astrocytes of the optic nerve (red arrows). (GFAP, x100 magnification). D3: Intensified axonal staining of NFP are seen in the optic nerve (red arrows) (NFP, x100 magnification). *C-G-MSC Group* E1: Histological sections of the optic nerve in the C-G-MSC group revealed vacuolization in myelin and degeneration in axons. E2: GFAP immunohistochemistry demonstrated glial hypertrophy with increased expression in glial cells of the optic nerve (red arrows). (GFAP, x100 magnification). E3: NFP immunohistochemistry shows enlarged axonal fibers with intense staining (red arrows) (NFP, x100 magnification).

Table 2
Statistical analysis of $CD90^{+}GFP^{+}$, $CD90^{+}Brn3a^{+}$, $Brn3a^{+}GFP^{+}$, $CD11b^{+}GFP^{+}$ and $CD11b^{+}Brn3a^{+}$ cells analyzed via flow cytometry.

Groups	$CD90^{+}Brn3a^{+}$	$Brn3a^{+}GFP^{+}$	$CD11b^{+}GFP^{+}$	$CD90^{+}GFP^{+}$
Control	1.30 ± 0.41	0.26 ± 0.07	0.17 ± 0.06	1.42 ± 0.27
G-SHAM	0.90 ± 0.05	0.11 ± 0.03	0.32 ± 0.02	1,38 ± 0.17
MSC	1.96 ± 0.03	0.34 ± 0.14	0.65 ± 0.08	2.48 ± 0.12 $^{**,++}$
G-MSC	4.26 ± 0.18 $^{***,++++,\#\#}$	1.08 ± 0.32 $^{*,+,\#}$	1.63 ± 0.15 $^{*,+,\#}$	2.35 ± 0.29 $^{*,++}$
C-G-MSC	3.89 ± 0.52 $^{**,++,\#}$	0.41 ± 0.16	0.64 ± 0.37	2.27 ± 0.08 $^{**,++}$

Values were given as mean ± standard deviation.
Control group (CONTROL), MSC group (MSC), Glaucoma-Sham group (G-SHAM), Glaucoma-MSC group (G-MSC), and Concurrent-Glaucoma-MSC group (C-G-MSC). Statistically significant differences were stated with signs; " * " compared to Control Group, and " + " compared to G-SHAM group, and "#" compared to MSC group. $^{*,+,\#}$; $p < 0.05$, $^{**,++,\#\#}$; $p < 0.01$, *** ; $p < 0.005$, $^{++++}$; $p < 0.001$.

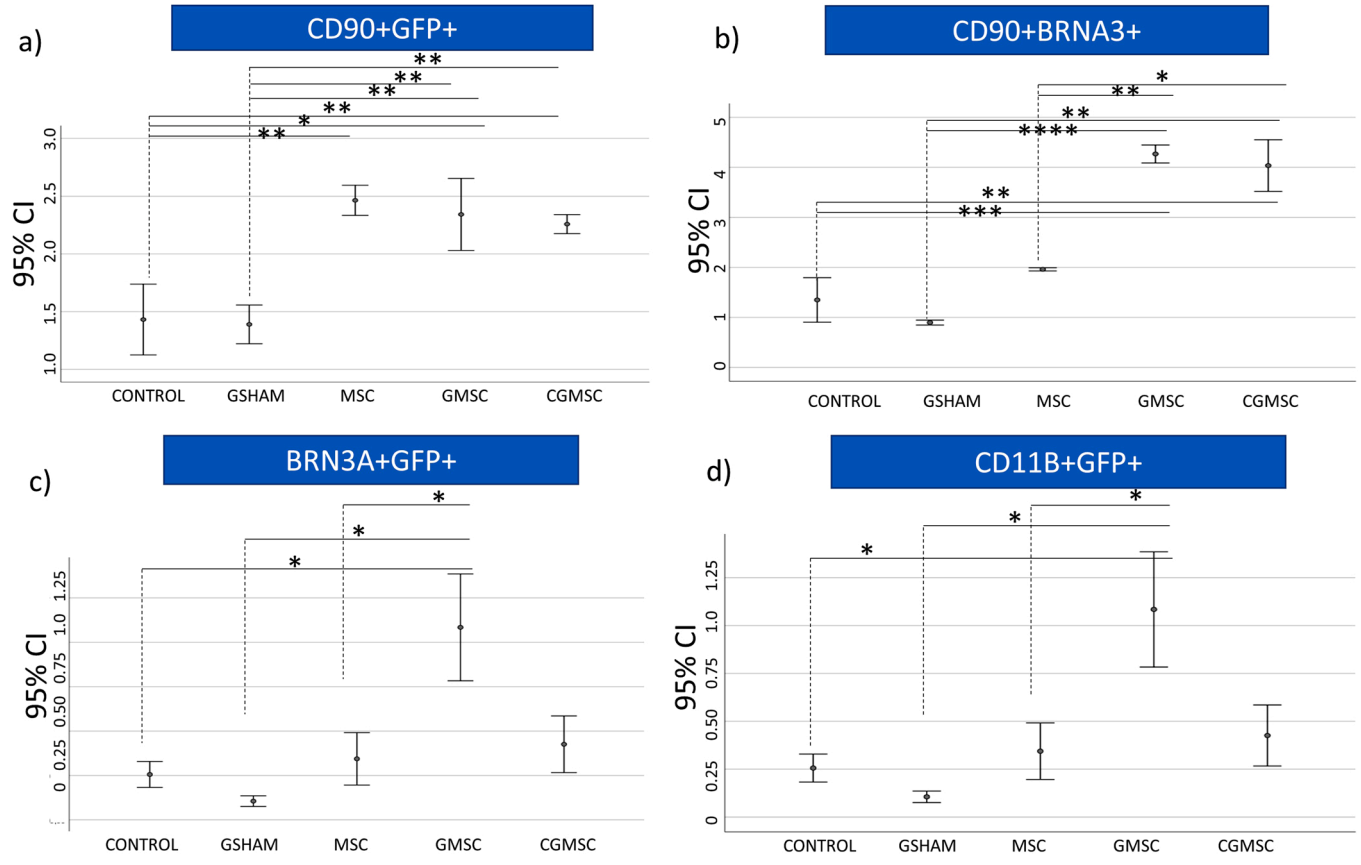

Fig. 4. The flow cytometry frequency of $CD90^{+}GFP^{+}$, $CD90^{+}Brn3a^{+}$, $Brn3a^{+}GFP^{+}$ and $CD11b^{+}GFP^{+}$ cells. a) Diagram showing $CD90^{+}GFP^{+}$ cells were significantly high in MSC, current-glaucoma-MSC (C-G-MSC) group, and glaucoma-MSC (G-MSC) treated groups. b) $CD90^{+}Brn3a^{+}$ cells significantly increased in C-G-MSC and G-MSC groups compared to the control group. A significant increase of $Brn3a^{+}GFP^{+}$ and $CD11b^{+}GFP^{+}$ cells in the G-MSC group is shown in figures c) and d).

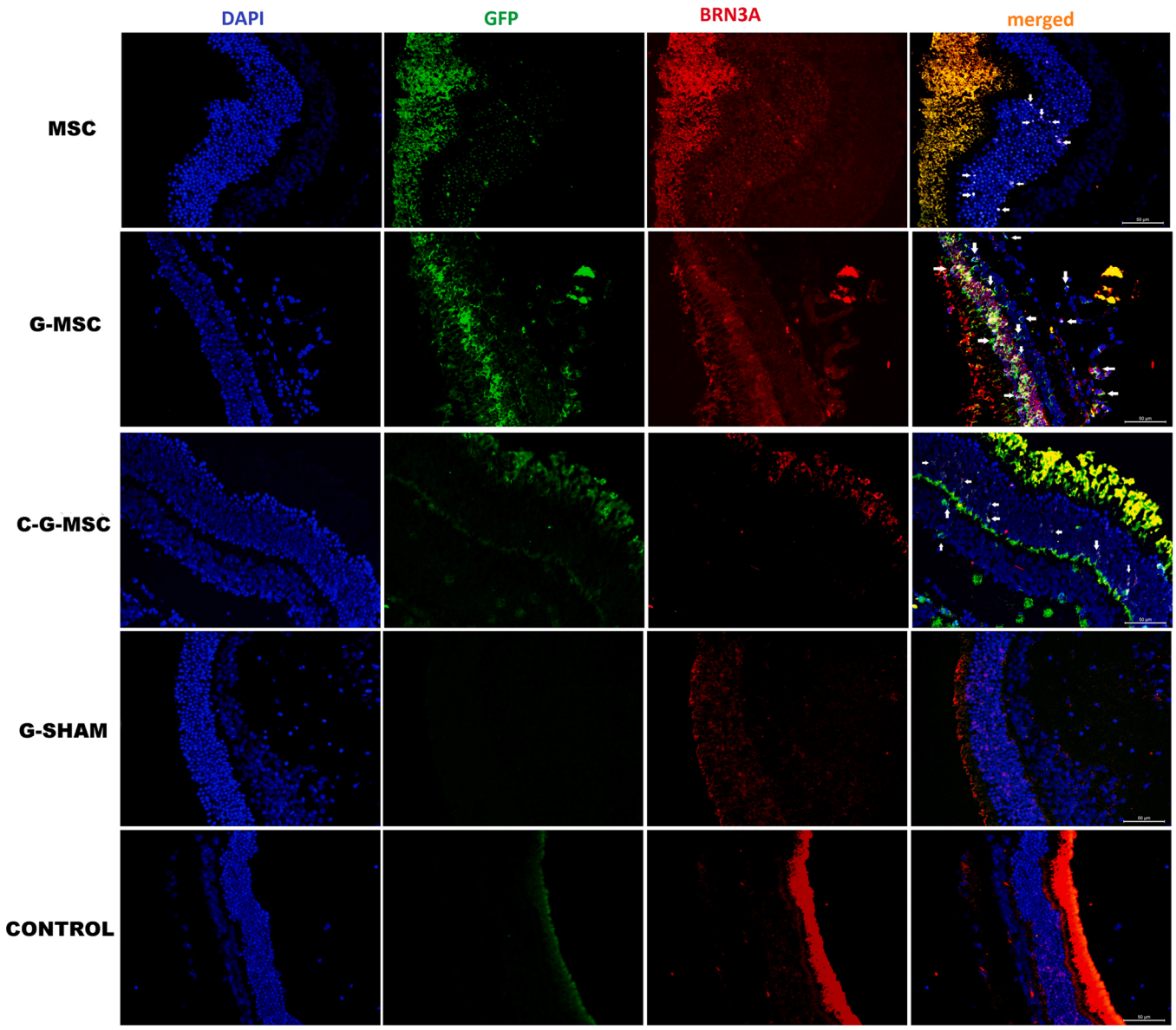

Fig. 5. Immunofluorescence staining of the retinal tissue sections. BRN3A (red) and GFP (green) antibodies were stained on tissue sections of all groups. GFP labeled MSCs were stained GFP positive (arrows) but control and G-SHAM groups were negative (Scale bars:50 μm).

GFP-labelled cells demonstrated the integration of rBM-MSCs into the retinal layers. When rBM-MSCs integrations were compared, the most intense migration was observed in the G-MSC group, followed by the C-G-MSC group and MSC groups, respectively. This result may indicate that rBM-MSCs activity and survival rate may increase under glaucoma-induced apoptosis. Our previous diabetic rat retinopathy study findings revealed similar results that rBM-MSCs were integrated mainly around the inner nuclear layer, ganglion cell layer, and scarcely at the outer nuclear layer in the diabetic rats rather than healthy controls (Cerman et al., 2016).

In a similar study conducted by Johnson et al. (2010), they applied laser photocoagulation to the trabecular network to create a glaucoma model and transplanted GFP-labelled rBM-MSCs into the vitreous cavity. They found that the stem cells had integrated into the nerve fiber and ganglion cell layers following the fifth week. In another similar study published by Emre et al. (2015), a rat glaucoma model was generated employing intracameral injection of hyaluronic acid into the anterior chamber. In that study, stem cells originating from rat bone marrow or adipose tissue were transplanted intravitreally. They found that a limited number of stem cells had integrated into the ganglion cell layer and the inner nuclear layer. The number of cells expressing pro-inflammatory cytokines (interferon-γ and tumor necrosis factor-α) decreased in the MSC-transferred group compared with that in the OHT group after four weeks. IL-1Ra and prostaglandin E2 receptor expressions were increased in the rat bone marrow-derived MSC group, but the increase was more significant in the rat adipose tissue-derived MSC group, which indicates a neuroprotective effect of MSC's in the rat OHT model. Their limitations were the need for invasive weekly anterior chamber injections of hyaluronic acid to obtain significant, sustained OHT, which may cause undesirable side effects such as corneal edema and inflammatory reactions (Urcola et al., 2006). The hypertensive effect of weekly injections of agents that block the aqueous outflow channels might be partly associated with inflammatory trabeculitis (Weber and Zelenak, 2001). In our study, we generated a glaucoma model using the model of Sappington et al. (2010) with an injection of small volumes of polystyrene microspheres into the anterior chamber to impede aqueous outflow and elevate IOP. Intracameral injection of this microbead seems to reveal the most reliable results and has the closest pathophysiology to the human OHT. This method has evolved as a preferred method of IOP elevation in rodents because of the sustained

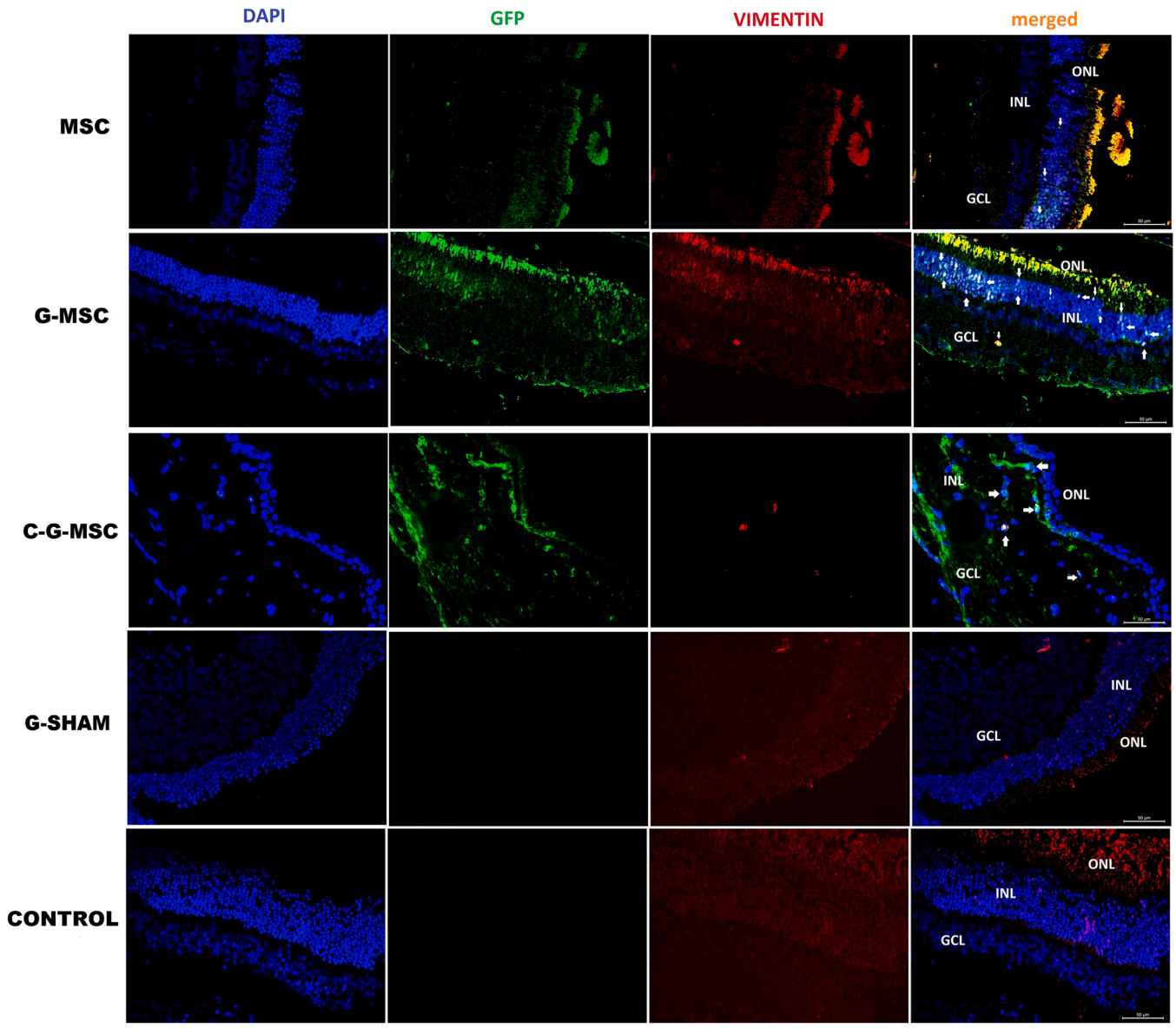

Fig. 6. Immunofluorescence staining of the retinal tissue sections. Vimentin (red) and GFP (green) antibodies were stained on tissue sections of all groups. GFP labeled MSCs were stained GFP positive (arrows) but control and G-SHAM groups were negative (Scale bars:50 μm).

and moderate elevation of intraocular pressure, which can be initiated at precise time points (Calkins et al., 2018; Morgan and Tribble, 2015). Both IOP magnitude and duration can be manipulated relatively simply with minimal confounding factors and internal control for each animal (Wareham et al., 2019; Sappington et al., 2010).

Flow cytometry results revealed that ganglion cell (Brn3a+) and glial cell (CD11b+) markers increased in the G-MSC and C-G-MSC groups. The markers of stem cells ($CD90^{+}GFP^{+}$) were significantly high in all rBM-MSCs applied groups. This result indicates that injected GFP labeled cells were located in rodent retinas. These results are similar to the findings of the previous studies (Cerman et al., 2016; Emre et al., 2015). The frequency of $Brn3a^{+}GFP^{+}$ and $CD11b^{+}GFP^{+}$ cells were notably increased in the G-MSC group compared to other groups ($P < 0.05$), but no significant difference was found when the C-G-MSC group was compared to MSC, G-Sham, or Control groups, respectively ($P > 0.05$). These results show that the viability and differentiation of MSCs into ganglion-like and microglia-like cells dependent on both implantation and the existence of apoptotic signals. This result is consistent with previous studies (Emre et al., 2015).

In another study conducted by Yu et al. (2006), labeled rBM-MSCs were observed in the nerve fiber and ganglion cell layers two weeks after transplantation. In the study of Emre et al. (2015), the GFP labeled rBM-MSCs traveled into the internal nuclear layer two and four weeks after transplantation. Unlike these previous studies, our present study revealed that the transplanted stem cells could reach the outer nuclear layer in a glaucoma model. Our previous electrophysiology study of diabetic rats with retinopathy revealed similarly that the transplanted stem cells may be located in the ganglion cell, inner nuclear, and outer nuclear layers and may differentiate to both ganglion and Müller like cells.

Yu et al. (2006) showed that intravitreally transplanted MSCs might have neuroprotective effects on RGC using secretion CNTF, GDNF, and other than the cell differentiation BDNF, and bFGF, in a glaucoma model, in which a 12-week glaucoma model. Emre et al. (2015) also demonstrated the presence of neuroprotective effects of MSCs on RGCs. They proposed that the action mechanism of stem cells in neuroprotection might be the secretion of neurotrophic factors like BDNF, GDNF, CNTF, and bFGF for modulation of inflammatory processes and inhibitory signals that regulate axonal re-growth along with neuronal repair and activation of endogenous repair mechanisms (Emre et al.,

2015).

There were some limitations of our study, including the need for a more extended time to observe the experimental model. The current established experimental model is an acute OHT model that mimics only some glaucoma features, such as pressure-induced RGC loss. However, chronicity, as seen in primary open-angle glaucoma, is not present in our acute experimental model (Moreno et al., 2005). In their recent report, Agudo-Barriuso et al. (2013) mentioned that increased IOP above normal levels induces apoptosis of RGCs, which occurs even if the IOP returns to basal values one week later. They emphasized that the injection-based OHT models, especially the microbead model, cause protracted damage to both inner and outer retinal layer neurons, as well as to RGCs and their axons. Urcola et al. suggested that injection-based methods are more appropriate for studying chronic IOP effects as the conclusion of their study. They compared three experimental glaucoma models in rats and revealed that IOP elevation and cell death in the OHT models were similar (Urcola et al., 2006).

In conclusion, we demonstrated that intravitreally transplanted rBM-MSCs might differentiate to ganglion-like cells in a rat experimental glaucoma model. It is possible to speculate that MSCs promise hope for glaucoma as neuro-regeneration therapies and that this approach can be a preferred method in the future. Long-term results must be determined to understand the side effects and to reveal the neuro-protective potential of MSCs.

5. Summary points

- Glaucoma is one of the significant causes of blindness.
- Glaucoma is regarded as progressive optic neuropathy, characterized by degeneration of retinal ganglion cells (RGCs) associated with elevated intraocular pressure (IOP).
- Mesenchymal stem cells (MSCs) are considered as multipotent adult progenitor cells and they have the capacity to self-renew and differentiate into various cell lineages.
- The differentiation of intravitreally injected rBM-MSCs to retinal ganglion-like cells in a rat glaucoma model induced with anterior chamber polystyrene microsphere injection.
- A total of 34 adult male Wistar albino rats with a bodyweight of about 200–250 g were used in the study.
- The right eyes of rats (n = 10) were used as the **Control group (CONTROL),** and the left eyes with induced OHT were enrolled into the **Glaucoma-Sham group (G-SHAM)**.
- The right eyes were called as **MSC group (n = 12) (MSC) and the left eyes as the Glaucoma-MSC group (G-MSC)**.
- OHT was induced at 14. day concurrently with rBM-MSCs transplantation in the left eyes and these eyes were labeled as the **Concurrent-Glaucoma-MSC group (C-G-MSC).**
- Intraocular pressure (IOP) increased significantly within 24 h following polystyrene microsphere injections into the anterior chamber until the end of the 2nd week.
- Glial cells in G-MSC group are found to be increased in number and distributed haphazardly throughout the optic nerve. GFAP immunohistochemistry demonstrated glial hypertrophy with increased expression in glial cells of the optic nerve. NFP immunohistochemistry shows enlarged axonal fibers with intense staining.
- The frequency of $Brn3a^{+}GFP^{+}$ and $CD11b^{+}GFP^{+}$ cells notably increased in the G-MSC group compared to the other groups.
- intravitreally transplanted rBM-MSCs might differentiate to ganglion-like cells in a rat experimental glaucoma model.

Ethical conduct of research

The study was granted by Marmara University, BAPKO (Scientific Research Project Commission), with project number SAG-B-120613–0239.

Financial & competing interests disclosure

The authors have no other relevant affiliations or financial involvement with any organization or entity with a financial interest in or financial conflict with the subject matter or materials discussed in the manuscript apart from those disclosed. No writing assistance was utilized in the production of this manuscript. All authors certify that they have no affiliations with or involvement in any organization or entity with any financial interest.

CRediT authorship contribution statement

M Eraslan, Tunc Akkoc and E Karaöz is responsible for the study conception and design. E Cerman, Tolga Akkoc, D Genc and S Bozkurt, supervised the sample collecting and murine studies; D Genc, AT Virlan and C Subası designed and supervised the experimental study. M Eraslan, Tunc Akkoc E Cerman and Tolga Akkoc contribute to manuscript writing. All authors read and approved the final manuscript. All authors read and approved the final version of the manuscript.

Declaration of Competing Interest

None of the authors have any proprietary interest or conflict of interest related to this submission.

Data Availability

No data was used for the research described in the article. Raw data were generated at Marmara University Faculty of Medicine. Derived data that support the findings of this study are available from the corresponding author (ME) on request.

References

Agudo-Barriuso, M., Villegas-Perez, M.P., de Imperial, J.M., Vidal-Sanz, M., 2013. Anatomical and functional damage in experimental glaucoma. Curr. Opin. Pharmacol. 13, 5–11.
Akkoc, T., Genc, D., 2020. Asthma immunotherapy and treatment approaches with mesenchymal stem cells. Immunotherapy 12, 665–674.
Aydin, R., Baris, M., Durmaz-Engin, C., Al-Aswad, L.A., Blumberg, D.M., Cioffi, G.A., Liebmann, J.M., Tezel, T.H., Tezel, G., 2021. Early localized alterations of the retinal inner plexiform layer in association with visual field worsening in glaucoma patients. PLoS One 16, e0247401.
Bunce, C., Wormald, R., 2006. Leading causes of certification for blindness and partial sight in England & Wales. BMC Public Health 6, 58.
Calkins, D.J., Lambert, W.S., Formichella, C.R., McLaughlin, W.M., Sappington, R.M., 2018. The microbead occlusion model of ocular hypertension in mice. Methods Mol. Biol. 1695, 23–39.
Cerman, E., Akkoc, T., Eraslan, M., Sahin, O., Ozkara, S., Vardar Aker, F., Subasi, C., Karaoz, E., Akkoc, T., 2016. Retinal electrophysiological effects of intravitreal bone marrow derived mesenchymal stem cells in streptozotocin induced diabetic rats. PloS One 11, e0156495.
Ding, D.C., Shyu, W.C., Lin, S.Z., 2011. Mesenchymal stem cells. Cell Transpl. 20, 5–14.
Emre, E., Yuksel, N., Duruksu, G., Pirhan, D., Subasi, C., Erman, G., Karaoz, E., 2015. Neuroprotective effects of intravitreally transplanted adipose tissue and bone marrow-derived mesenchymal stem cells in an experimental ocular hypertension model. Cytotherapy 17, 543–559.
Esen, F., Kostek, M., Emekli, A.S., Eraslan, M., 2016. Double-organ bias in published randomized controlled trials of glaucoma. J. Glaucoma 25, 520–522.
Girdlestone, J., 2016. Mesenchymal stromal cells with enhanced therapeutic properties. Immunotherapy 8, 1405–1416.
Gordon, M.O., Kass, M.A., 2018. What we have learned from the ocular hypertension treatment study. Am. J. Ophthalmol. 189, xxiv–xxvii.
Hau, S., Bunce, C., Barton, K., 2021. Corneal endothelial cell loss after baerveldt glaucoma implant surgery. Ophthalmol. Glaucoma 4, 20–31.
Jin, G.Z., Cho, S.J., Choi, E.G., Lee, Y.S., Yu, X.F., Choi, K.S., Yee, S.T., Jeon, J.T., Kim, M. O., Kong, I.K., 2008. Rat mesenchymal stem cells increase tyrosine hydroxylase expression and dopamine content in ventral mesencephalic cells in vitro. Cell Biol. Int. 32, 1433–1438.
Johnson, T.V., Bull, N.D., Hunt, D.P., Marina, N., Tomarev, S.I., Martin, K.R., 2010. Neuroprotective effects of intravitreal mesenchymal stem cell transplantation in experimental glaucoma. Invest. Ophthalmol. Vis. Sci. 51, 2051–2059.
Joyce, N., Annett, G., Wirthlin, L., Olson, S., Bauer, G., Nolta, J.A., 2010. Mesenchymal stem cells for the treatment of neurodegenerative disease. Regen. Med. 5, 933–946.

Khine, K.T., Albini, T.A., Lee, R.K., 2020. Chronic retinal detachment and neovascular glaucoma after intravitreal stem cell injection for Usher Syndrome. Am. J. Ophthalmol. Case Rep. 18, 100647.
Kim, Y.J., Park, H.J., Lee, G., Bang, O.Y., Ahn, Y.H., Joe, E., Kim, H.O., Lee, P.H., 2009. Neuroprotective effects of human mesenchymal stem cells on dopaminergic neurons through anti-inflammatory action. Glia 57, 13–23.
Krabbe, C., Zimmer, J., Meyer, M., 2005. Neural transdifferentiation of mesenchymal stem cells–a critical review. APMIS 113, 831–844.
Lai, T.Y., Chen, L.J., Yam, G.H., Tham, C.C., Pang, C.P., 2010. Development of novel drugs for ocular diseases: possibilities for individualized therapy. Per. Med. 7, 371–386.
Laing, A.G., Riffo-Vasquez, Y., Sharif-Paghaleh, E., Lombardi, G., Sharpe, P.T., 2018. Immune modulation by apoptotic dental pulp stem cells in vivo. Immunotherapy 10, 201–211.
Liu, Y., Wang, J., Jin, X., Xin, Z., Wu, X., Tong, X., Tao, Y., Wang, D., 2020. A novel rat model of ocular hypertension by a single intracameral injection of cross-linked hyaluronic acid hydrogel (Healaflow((R)). Basic Clin. Pharm. Toxicol. 127, 361–370.
Mohammadzadeh, V., Su, E., Heydar Zadeh, S., Law, S.K., Coleman, A.L., Caprioli, J., Weiss, R.E., Nouri-Mahdavi, K., 2021. Estimating ganglion cell complex rates of change with bayesian hierarchical models. Transl. Vis. Sci. Technol. 10, 15.
Moreno, M.C., Marcos, H.J., Oscar Croxatto, J., Sande, P.H., Campanelli, J., Jaliffa, C.O., Benozzi, J., Rosenstein, R.E., 2005. A new experimental model of glaucoma in rats through intracameral injections of hyaluronic acid. Exp. Eye Res 81, 71–80.
Morgan, J.E., Tribble, J.R., 2015. Microbead models in glaucoma. Exp. Eye Res. 141, 9–14.
Ngumah, Q.C., Buchthal, S.D., Dacheux, R.F., 2006. Longitudinal non-invasive proton NMR spectroscopy measurement of vitreous lactate in a rabbit model of ocular hypertension. Exp. Eye Res. 83, 390–400.
Pang, I.H., Clark, A.F., 2007. Rodent models for glaucoma retinopathy and optic neuropathy. J. Glaucoma 16, 483–505.
Parr, A.M., Tator, C.H., Keating, A., 2007. Bone marrow-derived mesenchymal stromal cells for the repair of central nervous system injury. Bone Marrow Transplant. 40, 609–619.
Puertas-Neyra, K., Usategui-Martin, R., Coco, R.M., Fernandez-Bueno, I., 2020. Intravitreal stem cell paracrine properties as a potential neuroprotective therapy for retinal photoreceptor neurodegenerative diseases. Neural Regen. Res. 15, 1631–1638.
Sappington, R.M., Carlson, B.J., Crish, S.D., Calkins, D.J., 2010. The microbead occlusion model: a paradigm for induced ocular hypertension in rats and mice. Invest. Ophthalmol. Vis. Sci. 51, 207–216.
Slavin, S., Kurkalli, B.G., Karussis, D., 2008. The potential use of adult stem cells for the treatment of multiple sclerosis and other neurodegenerative disorders. Clin. Neurol. Neurosurg. 110, 943–946.
Torrente, Y., Polli, E., 2008. Mesenchymal stem cell transplantation for neurodegenerative diseases. Cell Transplant. 17, 1103–1113.
Urcola, J.H., Hernandez, M., Vecino, E., 2006. Three experimental glaucoma models in rats: comparison of the effects of intraocular pressure elevation on retinal ganglion cell size and death. Exp. Eye Res. 83, 429–437.
Usategui-Martin, R., Fernandez-Bueno, I., 2021. Neuroprotective therapy for retinal neurodegenerative diseases by stem cell secretome. Neural Regen. Res 16, 117–118.
Vercelli, A., Mereuta, O.M., Garbossa, D., Muraca, G., Mareschi, K., Rustichelli, D., Ferrero, I., Mazzini, L., Madon, E., Fagioli, F., 2008. Human mesenchymal stem cell transplantation extends survival, improves motor performance and decreases neuroinflammation in mouse model of amyotrophic lateral sclerosis. Neurobiol. Dis. 31, 395–405.
Wareham, L.K., Dordea, A.C., Schleifer, G., Yao, V., Batten, A., Fei, F., Mertz, J., Gregory-Ksander, M., Pasquale, L.R., Buys, E.S., Sappington, R.M., 2019. Increased bioavailability of cyclic guanylate monophosphate prevents retinal ganglion cell degeneration. Neurobiol. Dis. 121, 65–75.
Weber, A.J., Zelenak, D., 2001. Experimental glaucoma in the primate induced by latex microspheres. J. Neurosci. Methods 111, 39–48.
Yang, J., Tezel, G., Patil, R.V., Wax, M.B., 2000. Flow cytometry for quantification of retrogradely labeled retinal ganglion cells by Fluoro-Gold. Curr. Eye Res. 21, 981–985.
Yap, T.E., Shamsher, E., Guo, L., Cordeiro, M.F., 2020. Ophthalmic research lecture 2018: DARC as a potential surrogate marker. Ophthalmic Res 63, 1–7.
Yoshii, C., Ueda, Y., Okamoto, M., Araki, M., 2007. Neural retinal regeneration in the anuran amphibian Xenopus laevis post-metamorphosis: transdifferentiation of retinal pigmented epithelium regenerates the neural retina. Dev. Biol. 303, 45–56.
Yu, S., Tanabe, T., Dezawa, M., Ishikawa, H., Yoshimura, N., 2006. Effects of bone marrow stromal cell injection in an experimental glaucoma model. Biochem. Biophys. Res. Commun. 344, 1071–1079.
Zappia, E., Casazza, S., Pedemonte, E., Benvenuto, F., Bonanni, I., Gerdoni, E., Giunti, D., Ceravolo, A., Cazzanti, F., Frassoni, F., Mancardi, G., Uccelli, A., 2005. Mesenchymal stem cells ameliorate experimental autoimmune encephalomyelitis inducing T-cell anergy. Blood 106, 1755–1761.
Zhang, J., Brodie, C., Li, Y., Zheng, X., Roberts, C., Lu, M., Gao, Q., Borneman, J., Savant-Bhonsale, S., Elias, S.B., Chopp, M., 2009. Bone marrow stromal cell therapy reduces proNGF and p75 expression in mice with experimental autoimmune encephalomyelitis. J. Neurol. Sci. 279, 30–38.
Zhao, C.P., Zhang, C., Zhou, S.N., Xie, Y.M., Wang, Y.H., Huang, H., Shang, Y.C., Li, W.Y., Zhou, C., Yu, M.J., Feng, S.W., 2007. Human mesenchymal stromal cells ameliorate the phenotype of SOD1-G93A ALS mice. Cytotherapy 9, 414–426.